



HAL
open science

On self-preservation and log-similarity in a slightly heated axisymmetric mixing layer

F. Thiesset, V. Schaeffer, L. Djenidi, R. A. Antonia

► **To cite this version:**

F. Thiesset, V. Schaeffer, L. Djenidi, R. A. Antonia. On self-preservation and log-similarity in a slightly heated axisymmetric mixing layer. *Physics of Fluids*, 2014, 26 (7), pp.075106. 10.1063/1.4890994 . hal-01660266

HAL Id: hal-01660266

<https://hal.science/hal-01660266>

Submitted on 28 Mar 2019

HAL is a multi-disciplinary open access archive for the deposit and dissemination of scientific research documents, whether they are published or not. The documents may come from teaching and research institutions in France or abroad, or from public or private research centers.

L'archive ouverte pluridisciplinaire **HAL**, est destinée au dépôt et à la diffusion de documents scientifiques de niveau recherche, publiés ou non, émanant des établissements d'enseignement et de recherche français ou étrangers, des laboratoires publics ou privés.

1 On self-preservation and log-similarity in a slightly heated axisymmetric mixing layer

2 F. Thiesset,¹ V. Schaeffer,¹ L. Djenidi,^{1, a)} and R. A. Antonia¹

3 *School of Engineering, University of Newcastle, NSW 2308 Callaghan,*

4 *Australia*

This paper reports an experimental investigation of self-preservation for one- and two-point statistics in a slightly heated axisymmetric mixing layer. Results indicate that the longitudinal velocity fluctuation u seems to approach self-preservation more rapidly than either the transverse velocity fluctuation v or the scalar fluctuation θ . The Reynolds number $Re_\delta = U_0\delta/\nu$ (U_0 being the jet inlet velocity and δ the momentum thickness) that ought to be achieved for the one-point statistics to behave in a self-similar fashion is assessed. Second, the relevance of different sets of similarity variables for normalizing the energy spectra and structure functions is explored. In particular, a new set of shear similarity variables, emphasizing the range of scales influenced by the mean velocity and temperature gradient, is derived and tested. Since the Reynolds number based on the Taylor microscale increases with respect to the streamwise distance, complete self-preservation cannot be satisfied; instead, the range of scales over which spectra and structure functions comply with self-preservation depends on the particular choice of similarity variables. A similarity analysis of the two-point transport equation, which features the large scale production term, is performed and confirms this. Log-similarity, which implicitly accounts for the variation of the Reynolds number, is also proposed and appears to provide a reasonable approximation to self-preservation, at least for u and θ .

5 PACS numbers: 47.27.-i, 47.27.wj, 01.50.Pa

^{a)}Electronic mail: Email address : Lyazid.Djenidi@newcastle.edu.au

6 I. INTRODUCTION

7 The hypothesis of self-preservation which assumes that the flow is governed by a single set
8 of length, velocity and scalar scales has been extensively applied for describing the spatio-
9 temporal evolution of some canonical turbulent flows. Among the literature, this hypothesis
10 has led to significant contributions to the study of homogeneous isotropic turbulence (Refs.
11 1–4 among others) and to scalar fluctuations evolving in isotropic turbulence (*e.g.* Refs.
12 5–9). Self-preservation has also been applied to homogeneous shear turbulence^{10,11}, wake
13 flows^{12–17}, turbulent jets^{13,18–22} and turbulent shear-layers^{23–27}. It is important to stress that
14 the quest for self-preserving solutions has motivated many aspects of research in turbulence
15 since it has the tremendous advantage of reducing partial differential equations to ordinary
16 differential equations.

17 Generally speaking, one-point statistics (mean values, Reynolds stress, etc) as well as
18 as two-point statistics (*e.g.* spectra or structure functions) can be studied under the con-
19 straints imposed by self-preservation. When applied to two-point statistics, complete self-
20 preservation implicitly suggests that all scales behave similarly. It is now well known that
21 this requires the Reynolds number R_λ based on the Taylor microscale λ (to be defined later)
22 and a typical fluctuation u' to be constant (see *e.g.* Refs. 2–4, and 21). Indeed, the con-
23 stancy of R_λ ensures that the ratios between the different length-scales (the integral scale,
24 the Taylor microscale, the Kolmogorov scale) and velocity scales (for instance the rms, the
25 Kolmogorov velocity, ...) are also constant^{8,21,22}. In such cases, *inner* scales (*e.g.* the Taylor
26 microscale or the Kolmogorov length-scale) can be used interchangeably with *outer* scales
27 (the integral length-scale for example) because they all behave similarly. This circumvents
28 the question of which are the most relevant similarity variables to be used for normaliza-
29 tion. The only flows for which this constraint is respected is the far field of the round jet
30 (at least along the axis), the far field of a cylinder wake (preliminary results gathered by
31 our group suggest that x/D , where D is the diameter of the cylinder, needs to exceed a
32 value of about 200 before R_λ is constant), and the initial period of decay of grid turbu-
33 lence at an infinitely large Reynolds number. Therefore, the range of flows complying with
34 self-preservation appears to be very limited especially since the third flow is unlikely to be
35 realizable.

36 For turbulent flows for which R_λ varies significantly, complete self-preservation, *i.e.* self-

37 similarity of spectra or correlation functions at all scales, cannot be satisfied. Consequently,
38 the range of scales satisfying self-preservation depends on the particular choice of similarity
39 variables (see *e.g.* Refs. 4, 8, and 9), and it appears that outer variables are relevant for
40 normalizing the large-scales whilst inner variables are likely to be appropriate at small-scales.
41 Therefore, performing a self-similarity analysis in flows where R_λ varies significantly remains
42 a challenging task.

43 On the other hand, log-similarity has been subsequently proposed as an alternative to the
44 classical picture of self-similarity. Log-similarity was first applied to temperature spectra in
45 Rayleigh-Bénard convection²⁸ and was shown to hold over an impressive range of Rayleigh
46 numbers. Nelkin²⁹ soon suggested the applicability of such a similarity for fully developed
47 homogeneous isotropic turbulence. The main theoretical arguments in favour of the plau-
48 sibility of log-similarity rely on a multifractal analysis^{28,30,31} and variational approaches of
49 small-scale intermittency³¹. Clearly, the relevance of such approaches when the Reynolds
50 number is only moderate remains somewhat debatable.

51 The main objective of the present study is to investigate in detail the accuracy with which
52 self-similarity is satisfied in a heated axisymmetric shear layer. In particular, the focus is on
53 the approach towards self-preservation for one-point statistics, velocity-temperature correla-
54 tions as well as two-point statistics such as spectra and structure functions. Both dynamical
55 and scalar fields are examined. Whilst the validity of self-preservation in the axisymmetric
56 shear layer does not need to be further demonstrated, it is of interest to extend the analysis
57 to higher-order statistics (up to the third-order), previous studies being usually limited to
58 first- and second-order statistics²³⁻²⁷. Note that the axisymmetric shear layer has been less
59 studied than the plane mixing layer for which extensive measurements of high-order statis-
60 tics and small-scale quantities have been performed for example by Refs. 32 and 33. In
61 addition, to the best of our knowledge, extending the study of self-preservation to two-point
62 statistics in the shear layer has not been attempted previously. This seems quite surprising,
63 given that the shear layer is an archetypal flow, which feels the presence of a strong shear
64 as well as a persisting organized motion²⁴. Consequently, this particular flow appears to be
65 nicely tailored for studying the interactions between different ranges of scales and how they
66 could reach a possible equilibrium. For example, it is of interest to assess the range of scales
67 directly influenced by the mean shear and the mean temperature gradient, how they differ
68 in behaviour with the small-scales and which quantities are relevant for normalizing them.

69 Moreover, the Reynolds number R_λ is known to increase with respect to the streamwise dis-
70 tance. The shear layer is thus perfectly suited for investigating the departure from complete
71 self-preservation associated with the spatial variation of R_λ . Further, the relevance of the
72 log-similarity, whose major advantage is to implicitly account for this variation, can also be
73 assessed.

74 This paper is organized as follows. The experimental apparatus is first outlined in §II.
75 Second, the approach towards self-similarity for one-point statistics is investigated in §III.
76 The analysis is further extended to two-point statistics in §IV. For this purpose, four different
77 sets of similarity variables are tested both analytically (§IV B) and experimentally (§IV C),
78 notably the shear similarity variables which are defined in §IV A. Log-similarity is then
79 applied to the experimental data in §IV D. Conclusions are finally drawn in §V

80 II. EXPERIMENTS

81 Experiments were performed in a mixing layer associated with a slightly heated round
82 jet. The jet facility has been described in detail for example in Refs. 21 and 34. The jet
83 nozzle has a diameter of $D = 55\text{mm}$, and the jet exit velocity U_0 was set to $12.3\text{m}\cdot\text{s}^{-1}$.
84 The corresponding Reynolds number $Re_D = U_0 D / \nu$ is 46,700 (ν is the kinematic viscosity).
85 Some measurements were carried out in the boundary layer at the jet exit and it was found
86 that the mean velocity was consistent with a Blasius profile (see Fig. 1(c)). The maximum
87 turbulence level in the boundary layer was found to be of about 3.5%, *i.e.* in the range of
88 typical experiments^{26,34,35}(see Fig. 1(c)). The air at the inlet of the centrifugal blower was
89 heated using an electrical fan heater. The jet facility was also completely lagged with a glass
90 wool layer covered with a metallic foil overlay to obtain a more uniform mean temperature
91 profile at the exit. The homogeneity of the temperature profile at the jet exit was checked
92 using a thermocouple and found to be within 10%. The temperature excess $\theta_0 \approx 15^\circ\text{C}$
93 on the jet centerline. The ratio Gr/Re_D^2 ($Gr = gD^3(\theta_0 + T_a)/\nu^2 T_a$ is the Grashof number
94 with T_a is the ambient absolute temperature and g the gravity acceleration) was about
95 3.5×10^{-3} indicating that temperature can be considered as a passive scalar, since buoyancy
96 is negligible. Simultaneous velocity and temperature measurements were performed at six
97 different downstream distances from the jet nozzle $1.5 \leq x/D \leq 4$ and for several transverse
98 positions traversing the shear layer.

99 The longitudinal U and transverse V velocity components in the x in y direction re-
100 spectively (Fig. 1(a)) were measured using a X-wire probe, consisting a two Wollaston
101 (Pt-10%Rh) wires of diameter $2.5\mu\text{m}$ and typical length of 0.5mm . The angle between the
102 two wires was chosen to be about 60° in order to capture high velocity angles that may
103 occur in this particular region of the flow (see Fig. 1(b)). The lateral separation between
104 the two wires were about 0.5mm . The hot-wires were operated by in-house constant tem-
105 perature anemometer at an overheat ratio of 1.5. The hot-wire voltages were corrected from
106 temperature variations using³⁶

$$E_c(t) = E_m(t) \left(\frac{T_w - T_{cal}}{T_w - T(t)} \right)^{1/2} \quad (1)$$

107 where E_c and E_m are the corrected and measured voltages respectively. T_w , T_{cal} and $T(t)$
108 are respectively the wire temperature, the air temperature during calibration and the air
109 temperature during measurements. Calibration was made *in situ* in the potential core of
110 the jet. The look-up table method³⁷⁻³⁹ was employed for calibrating the X-wire probe with
111 velocity magnitudes in the range $0-30\text{m.s}^{-1}$ with velocity increments of 1m.s^{-1} and angles
112 in the range $\pm 60^\circ$ with increments of 10° .

113 A Wollaston (Pt) wire of nominal diameter $d_w = 0.6\mu\text{m}$, operated by in-house constant
114 current circuits, was used for temperature measurements. The current supplied to the wire
115 was 0.1mA , so that the wire was essentially insensitive to the flow velocity. The wire was
116 etched for a length $l_w \approx 0.6\text{mm}$, yielding a ratio l_w/d_w of about 1000. A square-wave injection
117 technique^{34,40} was adopted for the determination of the frequency response of the cold wire.
118 As emphasized in Fig. 1(d), the Pt- $0.6\mu\text{m}$ wire was chosen since the cut-off frequency f_c was
119 found to be larger than for a Pt-10%Rh- $0.63\mu\text{m}$ wire. The instantaneous temperature signal
120 is then corrected following the method of Ref. 43. The cut-off frequency was first fitted using
121 the functional $f_c = 1/2\pi\tau_w = A_1 + A_2\sqrt{U_0} + A_3U_0$, which allows to compute the instantaneous
122 time constant $\tau_w(t)$ knowing the instantaneous velocity magnitude $\sqrt{U^2(t) + V^2(t)}$. The
123 corrected temperature θ is then calculated from measured temperature θ_m following $\theta =$
124 $\theta_m + \tau_w(t)\partial\theta_m/\partial t$. The correction method of Ref. 40 was also tested and led to some very
125 similar corrections for the temperature signal and related statistics. The cold-wire probe has
126 an angle of 30° with the X-wire probe, the latter being aligned with the jet axis (Fig. 1(b)).
127 The cold-wire is displaced by about 0.7mm from the hot-wires in order to avoid interferences
128 (Fig. 1(b)).

129 The output signals from anemometer channels, operating the cold and hot wires, were
 130 passed through buck-and-gain circuits and low-pass filtered at a frequency f_c slightly larger
 131 than the Kolmogorov frequency $f_K = \bar{U}/2\pi\eta_K$ (\bar{U} is the mean velocity and η_K the Kol-
 132 mogorov length-scale to be defined later). The signals were acquired using a National in-
 133 strument 16 bits A/D converter at a sampling frequency $f_s = 2f_c$. Convergence of velocity
 134 and scalar statistics was checked and found to be satisfactory. The high turbulence level
 135 in the shear layer can significantly alter the reliability of the classical Taylor hypothesis
 136 $x \equiv \bar{U}t$. Therefore, for calculating two-point statistics, a local convection velocity is used in
 137 the Taylor hypothesis; for this purpose we followed the same procedure as outlined in Ref.
 138 [21](#).

139 III. SELF-PRESERVATION OF ONE-POINT STATISTICS

140 We first pay particular attention to the approach towards self-preservation for one-point
 141 statistics. At this stage, the relevant scales are the inlet velocity U_0 for the velocity field,
 142 the temperature excess $\theta_0 = T(y=0) - T_a$ for the temperature field, whilst the normalized
 143 transverse coordinate ξ is given by

$$\xi = -\frac{y - y_{0.5}}{\delta}. \quad (2)$$

144 $y_{0.5}$ is the position y where the longitudinal mean velocity \bar{U} is equal to $U_0/2$ (hereafter, the
 145 overbar denotes time averaged values) and the momentum thickness δ is defined by

$$\delta = \int_0^\infty \frac{\bar{U}(y)}{U_0} \left(1 - \frac{\bar{U}(y)}{U_0}\right) dy. \quad (3)$$

146 δ can be used interchangeably with the shear-layer thickness $\delta_{0.1} = y_{0.9} - y_{0.1}$ ($y_{0.9}$ and
 147 $y_{0.1}$ are the transverse locations where \bar{U}/U_0 is 0.1 and 0.9 respectively) and the vorticity
 148 thickness δ_ω

$$\delta_\omega = \frac{U_0}{\max\left(\frac{\partial\bar{U}}{\partial y}\right)} \quad (4)$$

149 since δ , $\delta_{0.1}$ and δ_ω all behave similarly with the downstream distance x . More precisely, all
 150 these length-scales are known to be proportional to x (*e.g.* Refs. [24](#), [26](#), and [35](#)).

151 Figs. [2\(a\)](#), [2\(b\)](#), [2\(c\)](#) present the first-, second- and third-order statistics of the velocity
 152 field normalized by the relevant quantities. A compilation of some published experimental

153 data are also given to assess the accuracy of the present measurements. Whilst the agreement
 154 between the present measurements and the published data of Refs. 35 and 44 is satisfactory
 155 for the mean velocity \overline{U}/U_0 , there are some slight differences as far as second-order statistics
 156 are concerned. These discrepancies may be first attributed to some differences in the initial
 157 conditions^{26,27,44}, especially the turbulence level which is slightly larger than that of Ref. 35.
 158 Second, and perhaps to a larger extent, these departures may be due to the particular probe
 159 used for measuring u and v (a 60° X-wire probe being likely to be more adequate than a
 160 45° in this region of the flow) and to the calibration method (the look-up table being more
 161 reliable than the yaw-angle method especially in highly turbulent flows³⁹).

162 It is observed that the longitudinal velocity component reaches a self-similar state rather
 163 quickly and there is a perfect collapse of both \overline{U}/U_0 and u'/U_0 (the prime stands for the
 164 rms value) for all the range of measurements $1.5D \leq x \leq 4D$ (only the range of $\xi \leq 3$ is
 165 considered for analysing self-similarity since for higher transverse distances, fluctuations in
 166 the potential core of the jet progressively increase). However, the collapse for the transverse
 167 velocity component v is attained less rapidly, and a distance of $x = 3.5D$ ($\equiv Re_\delta = U_0\delta/\nu =$
 168 6.4×10^3) has to be reached for v'/U_0 to behave in a self-similar fashion. This remark holds
 169 also for the Reynolds stress \overline{uv}/U_0^2 and higher-order statistics such as the kinetic energy flux
 170 $(\overline{vu^2} + \overline{v^3})/U_0^3$. Note that some measurements at a larger distance from the jet nozzle would
 171 have been necessary to confirm this since the assessment of self-similarity relies only on the
 172 two profiles at $x = 3.5D$ and $4D$. However, the present measurements seem to indicate that
 173 a Reynolds number $Re_\delta = 6.4 \times 10^3$ has to be attained for self-preservation to be satisfied
 174 for all velocity components. In Ref. 35, it was observed that v'/U_0 was self-similar beyond
 175 $x = 0.71D$ (no measurements were made at smaller distances) corresponding to $Re_\delta \approx 10^4$
 176 which is consistent with our observation. Noticeable is the fact that the maximum value
 177 for both v'/U_0 and \overline{uv}/U_0^2 progressively decreases before reaching its self-similar value of
 178 about 0.14 and -0.01 respectively. This may be associated with the presence of coherent
 179 structures, known as the Kelvin-Helmholtz vortices²⁴, whose energetic contribution to v'
 180 and \overline{uv} decreases as x increases. This point will be further confirmed when analysing two-
 181 point statistics.

182 The downstream evolution of the shear layer characteristic length-scales δ , $\delta_{0,1}$ and δ_ω is
 183 plotted in Fig. 2(d), together with their respective linear fit. The proportionality between δ ,
 184 $\delta_{0,1}$ and δ_ω and the streamwise distance x is well verified for the present measurements. The

185 slope for $\partial\delta/\partial x$ is equal to 0.0394 which is slightly larger than the commonly encountered
 186 values generally in the range $[0.029-0.037]$ ^{26,27}. $\partial\delta_{0.1}/\partial x = 0.185$ which is comparable with
 187 some published values $[0.17-0.23]$ (Ref. 26 and references therein). $\partial\delta_\omega/\partial x = 0.153$ in
 188 agreement with the data of Brown and Roshko²⁴ $[0.145 - 0.22]$. The linearity of δ , $\delta_{0.1}$ and
 189 δ_ω with x confirms that they can be used interchangeably for normalizing the transverse
 190 distance y .

191 We now turn our attention to the scalar field. For convenience, the temperature excess θ
 192 relative to the ambient temperature T_a is considered here, viz. $\theta = T - T_a$. Experimental data
 193 for the mean scalar value $\bar{\theta}$, and the rms of scalar fluctuations θ' , the velocity-temperature
 194 correlations $\overline{u\theta}$, $\overline{v\theta}$ and the temperature flux $\overline{v\theta^2}$, normalized by the appropriate set of simi-
 195 larity variables (the temperature excess $\Delta\theta_0 = T(y=0) - T_a$ and the momentum thickness
 196 δ), are given in Fig. 3(a), 3(b), 3(c) and 3(d) respectively. Even though comparing the
 197 plane and axisymmetric shear layer may be rather misleading, the mean temperature profile
 198 we obtain is roughly consistent with that inferred from Ref. 45. The mean and fluctu-
 199 ating temperature fields (Fig. 3(a) and 3(b)) appear to reach a self-similar state around
 200 $x = 3.5D$, *i.e.* at the same position as the transverse velocity component. The velocity-
 201 temperature correlations $\overline{u\theta}$ and $\overline{v\theta}$ (Fig. 3(c)) appear to be of opposite sign and also attain
 202 self-preservation at a streamwise distance of $x = 3.5D$. The transverse temperature flux,
 203 *i.e.* the transport of temperature fluctuations θ^2 by the transverse velocity component v is
 204 represented in Fig. 3(d). Here again, the profiles are roughly consistent with self-similarity
 205 for downstream distance $x \geq 3.5D$.

206 In summary, one-point statistics of the velocity components u, v and the scalar field θ
 207 reach a self-preserving state following different approaches. It is observed that statistics
 208 of u attain self-similarity more rapidly than that of v and θ . Arguably, this difference in
 209 behaviour is likely to be attributed to the contribution of the coherent motion which is
 210 mostly visible on v and diminishes with the streamwise distance. This statement can be
 211 further confirmed using energy spectra and structure functions on which we now turn our
 212 attention.

213 IV. SELF-PRESERVATION OF TWO-POINT STATISTICS

214 Extending the analysis of self-preservation to two-point statistics provides a deeper insight
 215 into the flow details since the evolution of the turbulence structure at a given scale can be
 216 assessed. In the present study, the relevance of four different sets of similarity variables for
 217 normalizing energy spectra and structure functions is tested

- 218 • The Kolmogorov variables⁴⁶ $u_K = (\nu\bar{\epsilon})^{1/4}$ and $\eta_K = (\nu^3/\bar{\epsilon})^{1/4}$ ($\bar{\epsilon} = 15\nu\overline{(\partial u/\partial x)^2}$ is the
 219 mean kinetic energy dissipation rate) for normalizing the velocity spectra and structure
 220 functions. For the temperature field, the Batchelor variables are used $\theta_B = \sqrt{\bar{\epsilon}_\theta\eta_K/u_K}$
 221 and $\eta_B = \eta_K/Pr$ (the Prandtl number $Pr = \nu/\kappa$ with κ the temperature diffusion
 222 coefficient and $\bar{\epsilon}_\theta = 3\kappa\overline{(\partial\theta/\partial x)^2}$ is the scalar dissipation rate).
- 223 • The George similarity variables², *i.e.* the velocity variance $\overline{u_\alpha^2}$ (u_α stands for either u or
 224 v) and the Taylor microscale $\lambda = \sqrt{15\nu\overline{u^2}/\bar{\epsilon}}$ for the velocity field and the temperature
 225 variance $\overline{\theta^2}$ and the Corrsin microscale $\lambda_\theta = \sqrt{3\kappa\overline{\theta^2}/\bar{\epsilon}_\theta}$ for the scalar field.
- 226 • The outer variables. The term "outer variables" should be understood as macroscopic
 227 scales, for instance δ is the characteristic length-scale and U_0 and θ_0 are used for
 228 normalizing the dynamical and scalar field respectively.
- 229 • The shear variables which are defined below.

230 A. Definition and assessment of the shear characteristic scales

231 In order to derive the shear characteristic scales, we will consider the simplified case of
 232 homogeneous shear turbulence. It is important to stress that this hypothesis might not be
 233 strictly applicable to the axisymmetric shear layer since *e.g.* the turbulent diffusion term
 234 is likely to contribute³² to the energy budget. However, it is obvious that the production
 235 mechanism associated with the mean shear is a predominant feature of the shear layer,
 236 especially at a transverse position $\xi = 0$ (see Ref. 32).

237 Let us first recall the arguments of Ref. 47 that allow to derive the shear length-scale for
 238 the dynamical field. In a turbulent flow dominated by the mean shear, the scale-by-scale

239 budget is given by¹¹

$$6\nu\frac{\partial(\overline{\Delta u})^2}{\partial r} - \overline{(\Delta u)^3} - \frac{6}{r^4} \int_0^r s^4 \overline{\Delta u \Delta v} S_u ds = \frac{4}{5} \bar{\epsilon} r. \quad (5)$$

240 $\Delta\beta = \beta(x+r) - \beta(x)$ is the velocity increment of the quantity $\beta \equiv u, v, \theta$ between two points
 241 separated by a distance r . The first term on LHS of Eq. (5) corresponds to the viscous
 242 term and dominates at rather small scales. The second term is identified as the non-linear
 243 transfer term whose contribution is mostly perceptible at intermediate scales. The third
 244 term corresponds to a production term through the mean velocity gradient $S_u = \partial\bar{U}/\partial y$
 245 and dominates at rather large scales^{11,47}. Casciola *et al.*⁴⁷ suggested that the shear length-
 246 scale L_S^u first defined on dimensional arguments by Corrsin⁴⁸ can be identified as the scale
 247 for which the production term in Eq. (5) balances the non-linear transfer term, *i.e.*

$$L_S^u \equiv r \text{ such as } \overline{(\Delta u)^3}(r) = \frac{6}{r^4} \int_0^r s^4 \overline{\Delta u \Delta v} S_u ds \quad (6)$$

248 Assuming $\overline{(\Delta u)^3} \propto \bar{\epsilon} r$ and $\overline{\Delta u \Delta v} \propto (\bar{\epsilon} r)^{2/3}$ (which strictly hold only at very high Reynolds
 249 numbers), one obtains

$$L_S^u = \sqrt{\frac{\bar{\epsilon}}{S_u^3}} \quad (7)$$

250 Then, from the one-point energy budget which features only the production and dissipation
 251 terms, one can write

$$U_S^2 S_u \sim \bar{\epsilon} \quad (8)$$

252 which leads to a shear characteristic velocity $U_S = \sqrt{\bar{\epsilon}/S_u}$. A similar analysis can be carried
 253 out for the scalar field by first recalling the scale-by-scale budget of $\overline{(\Delta\theta)^2}$ in presence a
 254 mean temperature gradient⁴⁹

$$2\kappa\frac{\partial(\overline{\Delta\theta})^2}{\partial r} - \overline{\Delta u (\Delta\theta)^2} - \frac{2}{r^2} \int_0^r s^2 \overline{\Delta v \Delta\theta} S_\theta ds = \frac{4}{3} \bar{\epsilon}_\theta r. \quad (9)$$

255 where $S_\theta = \partial\bar{\theta}/\partial y$ is the mean temperature gradient. Assuming $\overline{\Delta u (\Delta\theta)^2} \propto \bar{\epsilon}_\theta r$ and $\overline{\delta u \delta\theta} \propto$
 256 $(\bar{\epsilon} r)^{1/3} (\bar{\epsilon}_\theta r)^{1/3} (\bar{\epsilon}_\theta/\bar{\epsilon})^{1/6}$, and identifying the scale L_S^θ for which the transfer term is equal to
 257 the production term, a shear length-scale for the scalar field can be similarly derived, *viz.*

$$L_S^\theta = \sqrt{\frac{\bar{\epsilon}_\theta^{-3/2}}{\bar{\epsilon}^{1/2} S_\theta^3}} \quad (10)$$

258 One can further write the one-point budget of the temperature variance in the following
 259 form

$$U_S \theta_S S_\theta \sim \bar{\epsilon}_\theta \quad (11)$$

260 yields a shear characteristic temperature $\theta_S = \bar{\epsilon}_\theta / S_\theta \sqrt{S_u / \bar{\epsilon}}$. L_S^u and L_S^θ allow to assess the
 261 range of scales which are in essence influenced by the presence of the mean shear and tem-
 262 perature gradient⁴⁷. For $r \geq L_S^u, L_S^\theta$, statistics of the velocity and scalar fields are dominated
 263 by production effects. On the other hand, the non-linearity of the cascade mechanism is
 264 supposed to be sufficiently strong for scales smaller than L_S^β to behave in a universal manner,
 265 independently of the large scales.

266 The shear characteristics scales are plotted in Fig. 4(a) and 4(b). We plot the ratios
 267 δ / L_S^u and δ / L_S^θ since L_S^u and L_S^θ tend to infinity when the mean velocity and temperature
 268 gradient goes to zero. For $-4 \leq \xi \leq 2$, both L_S^u and L_S^θ are proportional to δ (see Fig. 4(a)),
 269 indicating that the shear length-scales are characteristic of rather large scale phenomena and
 270 fall into our definition of outer length-scales. The proportionality of L_S^u and L_S^θ to δ is simply
 271 related to the fact that $\bar{\epsilon} U_0^3 / \delta$ and $\bar{\epsilon}_\theta U_0 \theta_0^2 / \delta$ behave in a self-similar fashion. The ratios δ / L_S^u
 272 and δ / L_S^θ are about 3 at $\xi = 0$. It thus appears that L_S^u and L_S^θ are slightly smaller than
 273 the shear layer momentum thickness δ . The characteristic velocity U_S and temperature
 274 θ_S are also presented in Fig. 4(b). Here again, all curves collapse reasonably well when
 275 normalized by U_0 and θ_0 , confirming that the shear characteristic scales can be identified as
 276 outer macro-scales.

277 B. A priori analysis of self-similarity for two-point statistics

278 The aim of this section is to analyse *a priori* the adequacy of the different similarity
 279 variables for normalizing two-point statistics. For this purpose, let us write second- and
 280 third-order structure functions in dimensionless form

$$\overline{(\Delta u)^2} = \mathcal{U}^2(x) f(r/\mathcal{L}) \quad (12a)$$

$$\overline{(\Delta u)^3} = \mathcal{U}^3(x) g(r/\mathcal{L}) \quad (12b)$$

$$\overline{(\Delta u \Delta v)} = \mathcal{U}^2(x) h(r/\mathcal{L}) \quad (12c)$$

281 Injecting Eqs. (12) into Eq. (5), yields

$$[2] \frac{f'}{\tilde{r}} + [F_1] \frac{g}{\tilde{r}} + [F_2] \frac{1}{\tilde{r}^5} \Gamma = [F_3] \quad (13)$$

282 where $\tilde{r} = r/\mathcal{L}$, the prime denotes differentiation with respect to \tilde{r} and $\Gamma = \int_0^{\tilde{r}} \tilde{s}^4 h d\tilde{s}$. The
 283 three functions appearing in Eq. (13) can be expressed as

$$F_1 = Re_{\mathcal{L}} = \frac{\mathcal{U}\mathcal{L}}{\nu} \quad (14a)$$

$$F_2 = Re_{\mathcal{L}} \frac{S_u \mathcal{L}}{\mathcal{U}} \quad (14b)$$

$$F_3 = \frac{4}{5} \frac{\bar{\epsilon} \mathcal{L}^2}{\nu \mathcal{U}^2} \quad (14c)$$

284 Complete self-similarity implies that all terms within brackets must behave similarly with
 285 x . Since one of them appears to be constant, then F_1 , F_2 and F_3 should be also constant.
 286 Performing a similarity analysis without presupposing any particular form for \mathcal{U} and \mathcal{L}
 287 inescapably leads to several possible solutions depending on the constants F_1 to F_3 used for
 288 deriving them. For example, using Eqs. (14a) and (14c) leads to the Kolmogorov scales as
 289 the relevant length-scales whilst the shear variables emerge from the use of Eqs. (14a) and
 290 (14b). However, none of them are suitable in terms of simultaneously satisfying all three
 291 constraints. This indicates that complete self-similarity cannot be satisfied in the shear layer.
 292 To further describe this, let us assess the range of scales satisfying self-similarity depending
 293 on the particular set of similarity variables that is chosen.

- 294 • The Kolmogorov scales η_K and u_K . Recalling that in the shear layer $\bar{\epsilon} \propto x^{-1}$, we
 295 obtain

$$F_1 = \frac{u_K \eta_K}{\nu} \propto x^0 \quad (15a)$$

$$F_2 = \frac{S_u \eta_K}{u_K} \propto x^{-1/2} \quad (15b)$$

$$F_3 = \frac{4}{5} \frac{\bar{\epsilon} \eta_K^2}{\nu u_K^2} \propto x^0 \quad (15c)$$

296 Therefore, Kolmogorov similarity will be satisfied only at small scales for which the
 297 production term can be neglected. Arguably, this could be respected for scales in the
 298 range $0 \leq r \lesssim L_S^u$.

- 299 • George similarity variables $\lambda \propto x^{1/2}$ and $u' \propto x^0$

$$F_1 = \frac{u' \lambda}{\nu} = R_\lambda \propto x^{1/2} \quad (16a)$$

$$F_2 = R_\lambda \frac{S_u \lambda}{u'} \propto x^0 \quad (16b)$$

$$F_3 = \frac{4}{5} \frac{\bar{\epsilon} \lambda^2}{\nu u'^2} \propto x^0 \quad (16c)$$

300 which indicates that George similarity is expected to be relevant for both very small
 301 and very large scales. However, some substantial departures from self-similarity are
 302 expected in the intermediate range where g is predominant.

- 303 • Outer similarity variables $\delta \propto x$ and U_0

$$F_1 = \frac{U_0 \delta}{\nu} \propto x^1 \quad (17a)$$

$$F_2 = \frac{U_0 \delta S_u \lambda}{\nu u'} \propto x^1 \quad (17b)$$

$$F_3 = \frac{4 \bar{\epsilon} \delta^2}{5 \nu U_0^2} \propto x^1 \quad (17c)$$

304 The use of outer similarity variable will be relevant for the range of scales over which
 305 the viscous term $2f'/\tilde{r}$ is negligible. This is expected to be respected for scales in the
 306 range $r_c \lesssim r \leq \infty$, where r_c is the cross-over length-scale between the viscous and
 307 inertial range, *viz.* $r_c/\eta_K \approx 30^{3/4}$ (see *e.g.* Ref. 4).

- 308 • Shear variables. Since $L_s^\theta \propto \delta$ and $U_S \propto U_0$, similar deductions can be drawn for the
 309 shear similarity variables.

310 An analogous analysis for Eq. (9), which is not reported here for the sake of clarity,
 311 leads to exactly the same conclusions. In summary, depending on the particular choice of
 312 similarity variables, the range of scales which satisfies self-preservation differs. The Kol-
 313 mogorov variables are expected to be relevant for small and intermediate scales, departure
 314 from self-similarity when using George variables are likely to be observed at intermediate
 315 scales whilst outer and shear characteristic scales are adequate for large and intermediate
 316 scales.

317 C. Similarity of energy spectra and structure functions

318 We first consider the degree with which energy spectra comply with self similarity when
 319 normalized by the four different sets of similarity variables presented in the previous section.
 320 In Figs. 5(a), 5(b), 5(c) and 5(d) are plotted energy spectra at $\xi \approx 0$ in the range $1.5D \leq$
 321 $x \leq 4D$. In Fig. 5(a), a comparison of present spectra with those of Ref. 33 at $R_\lambda = 330$
 322 is given. The agreement at intermediate and small scales is almost perfect over two decades
 323 thus validating the present assessment of the energy spectra.

324 When velocity and temperature spectra are normalized by Kolmogorov and Batchelor
325 scales respectively (Fig. 5(a)), one observes a perfect collapse for the dissipative scales
326 up to the inertial range (strictly the restricted scaling range notwithstanding the quite
327 low Reynolds number of the flow). Altogether, self-similarity is satisfied for wavenumbers
328 $k\eta_{K,B} \geq 2 \times 10^{-2}$. For wavenumbers $k\eta_{K,B} < 10^{-2}$, there is a systematic increase in the
329 amplitude of the spectra with x . This is explained by the non-constancy of the Reynolds
330 number based on the Taylor microscale $R_\lambda = u'\lambda/\nu$ which increases from about 210 to 300
331 for $1.5 \leq x/D \leq 4$ (see *e.g.* Refs. 4, 8, and 9). Note also that the range of wavenumbers
332 over which spectra of u and θ satisfy self-similarity is wider than that of v . A peak in the v
333 spectra is easily discernible around $k\eta_K \sim 10^{-2}$, which progressively diminishes in amplitude
334 as x increases. At $x = 3.5D$ the spectrum of v follows closely that at $x = 4.0D$. The peak
335 in the v spectrum is a footprint of the organized motion which monotonically shrinks as
336 x increases. The peak ceases to be discernible for $x \geq 3.5D$. Arguably, the delay in the
337 approach towards self-preservation for v that was observed for one-point statistics is likely
338 to be due to these coherent structures and more particularly to the time they need before
339 reaching a quasi-equilibrium state.

340 When using the George similarity variables² (see Fig. 5(b)), the collapse is satisfactory
341 notwithstanding the slightly larger scatter in the inertial range. For v , a significant departure
342 is also observed in the dissipative range. This differs from what is generally observed for
343 example in grid^{4,8,9} or wake turbulence¹⁷. In these flows, it is generally observed than
344 the George similarity² is satisfied over a wider range of scales than with the Kolmogorov
345 similarity. Here again, this feature is simply related to the Reynolds number R_λ which
346 substantially increases (by a factor 1.5) between $x = 1.5D$ and $x = 4D$.

347 Spectra normalized by the outer similarity variables δ , U_0 and θ_0 are presented in Fig.
348 5(c). In contrast to the Kolmogorov or George similarity variables, the outer scales lead to
349 a satisfactory collapse for the large-scales, including also a part of the pseudo-inertial range.
350 However, there is a significant drift towards high wavenumbers as x increases. In addition
351 to the similarity analysis as provided in §IV B, this feature can be further explained by first
352 recalling the definition of the normalized dissipation rate C_ϵ

$$\bar{\epsilon} = C_\epsilon \frac{U_0^3}{\delta} = \frac{C_\epsilon}{A_I^3} \frac{u'^3}{\delta} \quad (18)$$

353 $A_I = u'/U_0$ and C_ϵ were verified to be constant with x (see Figs. 2(b) and 4(a) for A_I and

354 C_ϵ respectively). Using Eq. (18) it can be shown that

$$\frac{\delta}{\lambda} = \frac{C_\epsilon}{15A_I^3} R_\lambda \quad (19a)$$

$$\frac{\delta}{\eta_K} = \frac{C_\epsilon}{A_I^3} 15^{-3/4} R_\lambda^{3/2} \quad (19b)$$

$$\frac{U_0^2}{u_K^2} = \frac{1}{A_I^2 \sqrt{15}} R_\lambda \quad (19c)$$

355 Therefore, since R_λ increases, then the ratios δ/λ and δ/η_K increase and hence the normal-
 356 ized spectra progressively drift towards high wavenumbers. Unsurprisingly, similar deduc-
 357 tions can be made when the shear length-scales are used for normalisation (Fig. 5(d)) since
 358 L_S^u and L_S^θ are both proportional to δ .

359 We now turn our attention to the accuracy of the self-preservation hypothesis for second-
 360 order structure functions $\overline{(\Delta\beta)^2}$ ($\beta \equiv u, v, \theta$). Whilst spectra and structure functions are
 361 simply related by

$$E_\beta(k) = \frac{\overline{\beta^2}}{\pi} \int_0^\infty \left(1 - \frac{\overline{(\Delta\beta)^2}}{2\overline{\beta^2}} \right) \cos(kr) dr, \quad (20)$$

362 their physical interpretation differs. Indeed, spectra strictly represent the energy density at
 363 a given wavenumber whereas structure functions are more likely to represent a cumulative
 364 energy distribution for scales $\leq r$ (*e.g.* Refs 50–52). Second, $E_\beta(k) = [\text{m}^3\text{s}^{-2}]$ whereas
 365 $\overline{(\Delta\beta)^2} = [\text{m}^2\text{s}^{-2}]$ which means that, in addition to a velocity scale, a length scale has to be
 366 invoked for normalizing the spectra which is not the case for structure functions. Therefore,
 367 it is of interest to further study the accuracy with which self-preservation is satisfied in
 368 physical space.

369 Second-order structure functions normalized by the four different sets of similarity vari-
 370 ables are plotted in Figs. 6(a), 6(b), 6(c) and 6(d). Also included in Fig. 6(a) are the
 371 DNS structure functions of u and θ (Refs. 53 and 54) for a plane mixing layer at a similar
 372 Reynolds number ($R_\lambda = 250$). In the intermediate range of scales, some very slight dif-
 373 ferences are discernible, which may be attributed to the differences in the initial/boundary
 374 conditions. However, the degree of agreement (especially in the dissipative range) is suffi-
 375 ciently satisfactory to unambiguously support the reliability of the present measurements.
 376 With Kolmogorov or Batchelor scales (Fig. 6(a)), one observes a perfect collapse for $\overline{(\Delta\beta)^2}$
 377 at rather small scales, *i.e.* from the dissipative range up to the middle of the pseudo-inertial
 378 range. This is absolutely consistent with our theoretical expectations performed in §IV B.

379 Here again, the range of r over which $\overline{(\Delta u)^2}$ and $\overline{(\Delta \theta)^2}$ satisfy self-preservation is wider
 380 than for $\overline{(\Delta v)^2}$. A hint of a bump is discernible in the structure function of v for scales
 381 $r \approx 3 \times 10^2$, highlighting the persisting influence of the coherent motion^{17,55,56}. With the
 382 George variables (Fig. 6(b)), in agreement with section §IV B, scatter is observed in the
 383 inertial range, especially for u and θ . As far as the transverse velocity component v is con-
 384 cerned, the departure from self-similarity surprisingly appears in dissipative range. This is
 385 most likely due to a bias when dividing $\overline{(\Delta v)^2}$ by $\overline{v^2}$, the latter being altered by the energy
 386 contribution of the coherent motion. As was observed in the energy spectra, the use of either
 387 outer-variable (Fig. 6(c)) or shear-variables (Fig. 6(d)) leads to a reasonable collapse from
 388 large down to intermediate scales, whereas in the dissipative range, the different curves tend
 389 to drift towards small-scales when x increases.

390 In summary, complete self-preservation, *i.e.* self-similarity of energy spectra and structure
 391 functions over the whole range of scales or wavenumbers, appears to be untenable since R_λ
 392 significantly increases with respect to the streamwise distance. As a consequence, the range
 393 of scales over which self-similarity is observed depends on the particular choice of similarity
 394 variables. Kolmogorov variables are suitable for small up to intermediate scales. A significant
 395 departure from self-similarity is observed in the inertial range when using George similarity
 396 whereas outer and shear variables are equally suitable for normalizing large and intermediate
 397 scales. These observations are in perfect agreement with the theoretical analysis presented
 398 in §IV B.

399 The fact that large and small-scales both satisfy self-similarity with an overlap at inter-
 400 mediate scales, if normalized by their respective relevant quantities, suggests that complete
 401 self-preservation could be plausible. If such a scaling exists, it would rely on a more sophisti-
 402 cated transformation than the one arising from a single set of similarity variables. Notably,
 403 such a scaling should account for the relative behaviour of the different similarity variables.
 404 The next section addresses this issue.

405 D. Log-similarity of energy spectra and structure functions

406 The main idea is to use both outer and inner variables in a single representation for energy
 407 spectra and structure functions. In other words, instead of invoking only **one** set of velocity,
 408 length, and scalar characteristic scales, a new type of normalization could be proposed using

409 **two** sets of similarity variables: one targeting the large-scales, the other the small-scales.
 410 Then one should define an appropriate transformation so that the relative behaviour between
 411 outer and inner scales is accounted for. One solution is a log-type similarity. This type of
 412 similarity solution is not new. It has been first observed and justified for the temperature field
 413 in a Rayleigh-Bénard convection flow²⁸ and further investigated in detail for the dynamical
 414 field in fully developed homogeneous isotropic turbulence^{29–31}.

415 Let us first define two functions $f_\delta^{u_\alpha}$ and $f_{\eta_K}^{u_\alpha}$ such as

$$f_\delta^{u_\alpha} = \frac{\log\left(C_1 \frac{(\overline{\Delta u_\alpha})^2}{U_0^2}\right)}{\log\left(\frac{U_0^2}{u_K^2}\right)} \quad (21a)$$

$$f_{\eta_K}^{u_\alpha} = \frac{\log\left(C_1 \frac{(\overline{\Delta u_\alpha})^2}{u_K^2}\right)}{\log\left(\frac{U_0^2}{u_K^2}\right)}. \quad (21b)$$

416 $f_\delta^{u_\alpha}$ and $f_{\eta_K}^{u_\alpha}$ ($u_\alpha \equiv u, v$) are respectively functions of r_δ and r_{η_K} defined by

$$r_\delta = \frac{\log\left(C_2 \frac{r}{\delta}\right)}{\log\left(\frac{\delta}{\eta_K}\right)} \quad (22a)$$

$$r_{\eta_K} = \frac{\log\left(C_2 \frac{r}{\eta_K}\right)}{\log\left(\frac{\delta}{\eta_K}\right)}. \quad (22b)$$

417 C_1 and C_2 are two constants. For the scalar field, similar definitions can be proposed

$$f_\delta^\theta = \frac{\log\left(C_1 \frac{(\overline{\Delta \theta})^2}{\Delta \theta_0^2}\right)}{\log\left(\frac{\Delta \theta_0^2}{\theta_B^2}\right)} \quad (23a)$$

$$f_{\eta_B}^\theta = \frac{\log\left(C_1 \frac{(\overline{\Delta \theta})^2}{\theta_B^2}\right)}{\log\left(\frac{\Delta \theta_0^2}{\theta_B^2}\right)} \quad (23b)$$

$$r_\delta = \frac{\log\left(C_2 \frac{r}{\delta}\right)}{\log\left(\frac{\delta}{\eta_B}\right)} \quad (23c)$$

$$r_{\eta_B} = \frac{\log\left(C_2 \frac{r}{\eta_B}\right)}{\log\left(\frac{\delta}{\eta_B}\right)}. \quad (23d)$$

418

419 From Eqs. (21a), (21b), (22a) and (22b), it can be shown that

$$f_\delta^{u_\alpha}(r_\delta) = f_{\eta_K}^{u_\alpha}(r_{\eta_K} - 1) - 1. \quad (24)$$

420 This very general identity holds for any set of similarity variables (as far as they are different)
421 and is not limited only to (δ, U_0) and (η_K, u_K) . Eq. (24) suggests that if $f_\delta^{u_\alpha}(r_\delta)$ is self-
422 similar, then so does $f_{\eta_K}^{u_\alpha}(r_{\eta_K})$ since they are related by a simple translation. Therefore,
423 this has the major advantage of circumventing the particular choice of similarity variables
424 that can be made for normalization and hence, a universal scaling independent of the sets
425 of similarity variables is likely to emerge. Similar definitions can be proposed for the energy
426 spectra

$$E_\delta^{u_\alpha} = \frac{\log\left(C_1 \frac{4\pi^2 E_{u_\alpha}}{U_0^2 \delta}\right)}{\log\left(\frac{U_0^2 \delta}{u_K^2 \eta_K}\right)} \quad (25a)$$

$$E_{\eta_K}^{u_\alpha} = \frac{\log\left(C_1 \frac{4\pi^2 E_{u_\alpha}}{u_K^2 \eta_K}\right)}{\log\left(\frac{U_0^2 \delta}{u_K^2 \eta_K}\right)}, \quad (25b)$$

$$E_\delta^\theta = \frac{\log\left(C_1 \frac{4\pi^2 E_\theta}{\Delta\theta_0^2 \delta}\right)}{\log\left(\frac{\Delta\theta_0^2 \delta}{u_B^2 \eta_B}\right)} \quad (25c)$$

$$E_{\eta_B}^\theta = \frac{\log\left(C_1 \frac{4\pi^2 E_\theta}{\theta_B^2 \eta_B}\right)}{\log\left(\frac{\Delta\theta_0^2 \delta}{u_B^2 \eta_B}\right)}, \quad (25d)$$

428

429 which are respectively functions of k_δ and $k_{\eta_{K,B}}$

$$k_\delta = \frac{\log(2\pi C_2 k \delta)}{\log\left(\frac{\delta}{\eta_{K,B}}\right)} \quad (26a)$$

$$k_{\eta_{K,B}} = \frac{\log(2\pi C_2 k \eta_{K,B})}{\log\left(\frac{\delta}{\eta_{K,B}}\right)}. \quad (26b)$$

430 Similarly, it is straightforward to show that

$$E_\delta^{u_\alpha}(k_\delta) = E_{\eta_K}^{u_\alpha}(k_{\eta_K} - 1) - 1. \quad (27)$$

431 The prefactor 2π in Eqs. (26a) and (26b) and the factor $4\pi^2$ in Eqs. (25a) and (25b)
432 arise from the definition of the wavenumber and the Fourier Transform respectively. It is
433 interesting to note that this log-similarity law is quite similar to the one proposed by Refs.
434 30 and 31. Indeed, using *e.g.* Eqs. (19c) and (19c), the expression for the energy spectra

435 can be recast as follows

$$E_\delta^{u_\alpha} \propto \frac{\log\left(\frac{E_{u_\alpha}}{E^\dagger}\right)}{\log\left(\frac{R_\lambda}{R^\dagger}\right)} \quad (28a)$$

$$k_\delta \propto \frac{\log\left(\frac{k}{k^\dagger}\right)}{\log\left(\frac{R_\lambda}{R^\dagger}\right)} \quad (28b)$$

436 where E^\dagger , R^\dagger and k^\dagger are some constants which are introduced here only for convenience.
 437 The log-similarity as given here by Eqs. (21a), (21b), (25a) and (25b) thus appears to be
 438 analogous to the log-similarity law proposed by Refs. 29–31.

439 The log-similarity has been tested using the present measurements and the results are
 440 presented in Figs. 7(a) and 7(b). With the exception of v for which, as already mentioned,
 441 the coherent motion contributes significantly to the energy distribution at large scales, the
 442 log-similarity law seems to be satisfied closely over the whole range of scales. Pragmatically
 443 speaking, this type of scaling acts as a compression-dilatation transformation of the spectra
 444 (or structure functions) and wavenumbers (or separations) so that they all fall onto a single
 445 curve. As a consequence, the analytical considerations of Refs. 30 and 31 on the basis of
 446 a multifractal analysis, are likely to apply here to theoretically justify the plausibility of a
 447 log-similarity in the axisymmetric mixing layer, albeit the quite low Reynolds number of the
 448 flow. The values for C_1 and C_2 were empirically assessed and set to 0.25 and 1 respectively.
 449 Further investigations are needed to provide a physical interpretation for these constants
 450 and to explore their dependence on the initial conditions, the Reynolds number and the
 451 type of flow.

452 V. CONCLUSION

453 Self-preservation for one- and two-point statistics in the slightly heated axisymmetric
 454 mixing layer of a round jet has been investigated by means of hot- and cold-wire anemometry.
 455 Special care has been paid to the reliability of the present measurements for which use was
 456 made of (i) a 60° X wire probe, calibrated by a look-up table method, to capture high velocity
 457 angles and high turbulence levels, (ii) a local convection velocity in Taylor’s hypothesis and
 458 (iii) an instantaneous correction method for the cold-wire time response.

459 Analysis of one-point statistics reveals that the dynamical and scalar fields follow different
 460 approaches towards self-similarity, the latter being reached more rapidly for u than for v

461 and θ . Altogether, all these quantities appear to attain a self-preserving state at $x = 3.5D$
462 corresponding to a Reynolds number Re_δ based on the upstream velocity U_0 and the shear
463 layer momentum thickness δ of 6.4×10^3 . It is clear that the approach to similarity of
464 v'/U_0 and \overline{wv}/U_0^2 is delayed relative to that for u'/U_0 . This is interpreted as being caused
465 by the footprint of coherent structures whose contribution is mostly perceptible on v and
466 progressively decreases as x increases. Spectra and structure functions of v corroborate this
467 interpretation.

468 Four different sets of similarity variables are tested for normalizing spectra and structure
469 functions. For this purpose, in addition to the scales L_S^u and U_S which pertain to the dynam-
470 ical field, a shear length-scale L_S^θ and characteristic temperature scale θ_S are introduced on
471 the basis of the scale-by-scale budget for the second-order temperature structure function.
472 L_S^u and L_S^θ allow the range of scales which is affected by the presence of the mean velocity
473 and temperature gradient, to be assessed. They are believed to be relevant quantities for a
474 slightly heated mixing layer. Experimental data reveal that the shear variables behave as
475 outer variables, *i.e.* L_S^u and L_S^θ are proportional to δ whilst U_S and θ_S scale as U_0 and θ_0
476 respectively. This is simply explained by the self-similar behaviour of the normalized mean
477 energy and scalar dissipation rates.

478 Since the Reynolds number R_λ increases significantly with the streamwise distance x ,
479 complete self-preservation is not attainable. Instead, the range of scales complying with self-
480 similarity depends on the particular choice of similarity variables. A similarity analysis of
481 the two-point transport equation featuring only the production term has been performed and
482 confirms this. Komogorov variables appear to be suitable at small and intermediate scales,
483 *i.e.* in the range $\eta_{K,B} \leq r \lesssim L_S^{u,\theta}$. George's similarity variables are adequate for normalizing
484 the very small- and very large-scales but there are significant departures at intermediate
485 scales where the non-linear energy transfer dominates. We noted also a bias, in the context
486 of George's similarity, associated with the non-negligible contribution of coherent motion to
487 the velocity variance. On the other hand, outer and shear variables lead to a satisfactory
488 collapse of spectra and structure functions at large and intermediate scales down to the
489 cross-over length-scale between viscous and inertial effects.

490 Log-similarity, which accounts for the variations of R_λ or equivalently the relative be-
491 haviour between outer and inner variables, has been introduced and tested. Instead of using
492 a single set of length, velocity or temperature characteristic scales for normalizing two-point

593 statistics, log-similarity relies on two sets of similarity variables. This has the major ad-
594 vantage of circumventing the particular choice of the two sets of similarity variables since it
595 was proven that *e.g.* $f_\delta(r_\delta)$ and $f_{\eta_K}(r_{\eta_K})$ are related by a simple translation transformation.
596 Results show that log-similarity applies for all scales with a very high degree of accuracy.
597 This observation opens the door to new perspectives for using the log-similarity hypothesis
598 in flows where R_λ varies such as grid turbulence in the initial period, the far field of a plane
599 jet or the intermediate wake region. However, whilst at very high Reynolds numbers, the
500 inertial range is sufficiently developed for log-similarity to be an intuitive or plausible scal-
501 ing, at low to moderate Reynolds numbers, there should be a limit in terms of variations
502 of R_λ for the log-similarity to be satisfied. Indeed, variations in curvature of second-order
503 structure functions (or spectra) in the pseudo-inertial range, which result from variations of
504 R_λ , are unlikely to be compensated indefinitely by a simple compression-dilatation transfor-
505 mation. The plausibility of the log-similarity in turbulence should further be demonstrated
506 on a dynamical basis (*i.e.* the scale-by-scale budget) rather than on phenomenological ar-
507 guments using multifractal models. These issues are left for future work. The two constants
508 C_1 and C_2 were introduced and assessed empirically. Further work is also needed to investi-
509 gate in detail their physical meaning and their dependence on the Reynolds number, initial
510 conditions or the type of flow.

511 ACKNOWLEDGMENTS

512 LD and RAA are grateful to the Australian Research Council for its support.

513 REFERENCES

- 514 ¹R. W. Stewart and A. A. Townsend, “Similarity and self-preservation in isotropic turbu-
515 lence,” [Phil. Trans. Roy. Soc. London](#) **243**, 359–386 (1951).
- 516 ²W. K. George, “The decay of homogeneous isotropic turbulence,”
517 [Phys. Fluids](#) **4**, 1492–1509 (1992).
- 518 ³C. G. Speziale and P. S. Bernard, “The energy decay in self-preserving isotropic turbulence
519 revisited,” [J. Fluid Mech.](#) **241**, 645–667 (1992).
- 520 ⁴R. A. Antonia, R. J. Smalley, T. Zhou, F. Anselmet, and L. Danaila, “Simi-

521 larity of energy structure functions in decaying homogeneous isotropic turbulence,”
522 [J. Fluid Mech.](#) **487**, 245–269 (2003).

523 ⁵W. K. George, “Self-preservation of temperature fluctuations in isotropic turbulence,” in
524 [Studies in Turbulence](#) (Springer, 1992) pp. 514–528.

525 ⁶J. R. Chasnov, “Similarity states of passive scalar transport in isotropic turbulence,”
526 [Phys. Fluids](#) **6**, 1036–1051 (1994).

527 ⁷M. Gonzalez and A. Fall, “The approach to self-preservation of scalar fluctuations decay
528 in isotropic turbulence,” [Physics of Fluids \(1994-present\)](#) **10**, 654–661 (1998).

529 ⁸R. A. Antonia and P. Orlandi, “Similarity of decaying isotropic turbulence with a passive
530 scalar,” [J. Fluid Mech.](#) **505**, 123–151 (2004).

531 ⁹R. A. Antonia, R. J. Smalley, T. Zhou, F. Anselmet, and L. Danaïla, “Similarity solu-
532 tion of temperature structure functions in decaying homogeneous isotropic turbulence,”
533 [Phys. Rev. E](#) **69**, 1–11 (2004).

534 ¹⁰W. K. George and M. M. Gibson, “The self-preservation of homogeneous shear flow tur-
535 bulence,” [Exp. Fluids](#) **13**, 229–238 (1992).

536 ¹¹L. Danaïla, F. Anselmet, and T. Zhou, “Turbulent energy scale-
537 budget equations for nearly homogeneous sheared turbulence,”
538 [Flow, Turbulence and Combustion](#) **72**, 287–310 (2004).

539 ¹²P. M. Bevilaqua and P. S. Lykoudis, “Turbulence memory in self-preserving wakes,”
540 [J. Fluid Mech.](#) **89**, 589–606 (1978).

541 ¹³W. K. George, “The self-preservation of turbulent flows and its relation to initial conditions
542 and coherent structures,” [Advances in Turbulence](#) , 39–74 (1989).

543 ¹⁴R. D. Moser, R. M. Moser, and D. W. Ewing, “Self-similarity of time-evolving plane
544 wakes,” [J. Fluid Mech.](#) **367**, 255–289 (1998).

545 ¹⁵R. A. Antonia and J. Mi, “Approach towards self-preservation of turbulent cylinder and
546 screen wakes,” [Exp. Therm. Fluid. Sci.](#) **17**, 277–284 (1998).

547 ¹⁶D. Ewing, W. K. George, M. M. Rogers, and R. D. Moser, “Two-point similarity in
548 temporally evolving plane wakes,” [J. Fluid Mech.](#) **577**, 287–307 (2007).

549 ¹⁷F. Thiesset, R. A. Antonia, and L. Danaïla, “Scale-by-scale turbulent energy budget in
550 the intermediate wake of two-dimensional generators,” [Phys. Fluids](#) **25**, 115105 (2013).

551 ¹⁸L. J. S. Bradbury, “The structure of a self-preserving turbulent plane jet,”
552 [J. Fluid Mech.](#) **23**, 31–64 (1965).

- 553 ¹⁹R. A. Antonia, B. R. Satyaprakash, and A. K. M. F. Hussain, “Measurements of
554 dissipation rate and some other characteristics of turbulent plane and circular jets,”
555 *Phys. Fluids* **23**, 695–700 (1980).
- 556 ²⁰D. Ewing, B. Frohnapfel, W. K. George, J. Pedersen, and J. Westerweel, “Two-point
557 similarity in the round jet,” *J. Fluid Mech.* **577**, 309–330 (2007).
- 558 ²¹P. Burattini, R. A. Antonia, and L. Danaila, “Similarity in the far field of a turbulent
559 round jet,” *Phys. Fluids* **17**, 025101 (2005).
- 560 ²²F. Thiesset, R. A. Antonia, and L. Djenidi, “Consequences of self-preservation on the axis
561 of a turbulent round jet,” *J. Fluid Mech.* **748**, R2 (2014).
- 562 ²³P. Bradshaw, “The effect of initial conditions on the development of a free shear layer,”
563 *J. Fluid Mech.* **26**, 225–236 (1966).
- 564 ²⁴G. L. Brown and A. Roshko, “On density effects and large structure in turbulent mixing
565 layers,” *J. Fluid Mech.* **64**, 775–816 (1974).
- 566 ²⁵H. E. Fiedler, “On turbulence structure and mixing mechanism in free turbulent shear
567 flows,” in *Turbulent mixing in nonreactive and reactive flows* (Springer, 1975) pp. 381–
568 409.
- 569 ²⁶A. K. M. F. Hussain and M. F. Zedan, “Effects of the initial condition on
570 the axisymmetric free shear layer: Effects of the initial momentum thickness,”
571 *Phys. Fluids* **21**, 1100–1112 (1978).
- 572 ²⁷A. K. M. F. Hussain and M. F. Zedan, “Effects of the initial condition on the axisymmetric
573 free shear layer: Effect of the initial fluctuation level,” *Phys. Fluids* **21**, 1475–1481 (1978).
- 574 ²⁸X.-Z. Wu, L. Kadanoff, A. Libchaber, and M. Sano, “Frequency power spectrum of
575 temperature fluctuations in free convection,” *Phys. Rev. Lett.* **64**, 2140–2143 (1990).
- 576 ²⁹M. Nelkin, “Multifractal scaling of velocity derivatives in turbulence,”
577 *Phy. Rev. A* **42**, 7226 (1990).
- 578 ³⁰U. Frisch and M. Vergassola, “A prediction of the multifractal model: the intermediate
579 dissipation range.” in *New Approaches and Concepts in Turbulence* (Springer, 1993) pp.
580 29–34.
- 581 ³¹B. Castaing, Y. Gagne, and M. Marchand, “Log-similarity for turbulent flows?”
582 *Physica D: Nonlinear Phenomena* **68**, 387–400 (1993).
- 583 ³²I. Wygnanski and H. E. Fiedler, “The two-dimensional mixing region,”
584 *J. Fluid Mech.* **41**, 327–361 (1970).

- 585 ³³F. H. Champagne, Y. H. Pao, and I. J. Wygnanski, “On the two-dimensional mixing
586 region,” *J. Fluid Mech.* **74**, 209–250 (1976).
- 587 ³⁴P. Burattini, R. A. Antonia, S. Rajagopalan, and M. Stephens, “Effect of initial conditions
588 on the near-field development of a round jet,” *Exp. Fluids* **37**, 56–64 (2004).
- 589 ³⁵A. K. M. F. Hussain and A. R. Clark, “On the coherent structure of the axisymmetric
590 mixing layer: a flow-visualization study,” *J. Fluid Mech.* **104**, 263–294 (1981).
- 591 ³⁶H. H. Bruun, *Hot wire anemometry : Principles and signal analysis* (Oxford University
592 Press, 1995).
- 593 ³⁷W. W. Willmarth and T. J. Bogar, “Survey and new measurements of turbulent structure
594 near the wall,” *Phys. Fluids* **20**, 9–21 (1977).
- 595 ³⁸R. M. Lueptow, K. S. Breuer, and J. H. Haritonidis, “Computer-aided calibration of
596 x-probes using a look-up table,” *Exp. Fluids* **6**, 115–118 (1988).
- 597 ³⁹P. Burattini and R. A. Antonia, “The effect of different x-wire schemes on some turbulence
598 statistics,” *Exp. Fluids* **38**, 80–89 (2005).
- 599 ⁴⁰J. Lemay and A. Benaïssa, “Improvement of cold-wire response for measurement of tem-
600 perature dissipation,” *Exp. Fluids* **31**, 347–356 (2001).
- 601 ⁴¹H. E. Fiedler, “On data acquisition in heated turbulent flows,” in
602 *Proceedings of the Dynamic Flow Conference 1978 on Dynamic Measurements in Unsteady Flows*
603 (Springer, 1978) pp. 81–100.
- 604 ⁴²R. A. Antonia, L. W. B. Browne, and A. J. Chambers, “Determination of time constants
605 of cold wires,” *Rev. Sci. Instrum.* **52**, 1382–1385 (1981).
- 606 ⁴³K. Bremhorst and L. J. W. Graham, “A fully compensated hot/cold wire
607 anemometer system for unsteady flow velocity and temperature measurements,”
608 *Meas. Sci. Technol.* **1**, 425–430 (1990).
- 609 ⁴⁴G. Xu and R. A. Antonia, “Effect of different initial conditions on a turbulent round free
610 jet,” *Exp. Fluids* **33**, 677–683 (2002).
- 611 ⁴⁵S. D. Rajagopalan and R. A. Antonia, “Properties of the large structure in a slightly
612 heated turbulent mixing layer of a plane jet,” *J. Fluid Mech.* **105**, 261–281 (1981).
- 613 ⁴⁶A. Kolmogorov, “The local structure of turbulence in incompressible viscous fluid for very
614 large Reynolds numbers,” *Proc. USSR Ac. of Sci.* **30**, 299–303 (1941).
- 615 ⁴⁷C. M. Casciola, P. Gualtieri, R. Benzi, and R. Piva, “Scale-by-scale budget and similarity
616 laws for shear turbulence,” *J. Fluid Mech.* **476**, 105–114 (2003).

- 617 ⁴⁸S. Corrsin, “Local isotropy in turbulent shear flow,” Tech. Rep. (NACA RM, 1958).
- 618 ⁴⁹L. Danaila and L. Mydlarski, “Effect of gradient production on scalar fluctuations in
619 decaying grid turbulence,” [Phys. Rev. E **64**, 016316 \(2001\)](#).
- 620 ⁵⁰A. A. Townsend, *The structure of turbulent shear flows*, edited by G. Batchelor (Cambridge
621 University Press, 1956).
- 622 ⁵¹P. A. Davidson and B. R. Pearson, “Identifying turbulent energy distributions in real,
623 rather than fourier, space,” [Phys. Rev. Lett. **95**, 214501 \(2005\)](#).
- 624 ⁵²H. Mouri and A. Hori, “Two-point velocity average of turbulence: Statistics and their
625 implications,” [Phys. Fluids **22**, 115110 \(2010\)](#).
- 626 ⁵³A. Attili and F. Bisetti, “Statistics and scaling of turbulence in a spatially developing
627 mixing layer at $Re_\lambda = 250$,” [Phys. Fluids **24**, 035109 \(2012\)](#).
- 628 ⁵⁴A. Attili and F. Bisetti, “Fluctuations of a passive scalar in a turbulent mixing layer,”
629 [Phys. Rev. E **88**, 033013 \(2013\)](#).
- 630 ⁵⁵F. Thiesset, L. Danaila, and R. A. Antonia, “Dynamical effect of the total strain induced
631 by the coherent motion on local isotropy in a wake.” [J. Fluid Mech. **720**, 393–423 \(2013\)](#).
- 632 ⁵⁶F. Thiesset, L. Danaila, and R. Antonia, “Dynamical interactions between the coherent
633 motion and small scales in a cylinder wake,” [J. Fluid Mech. **749**, 201–226 \(2014\)](#).

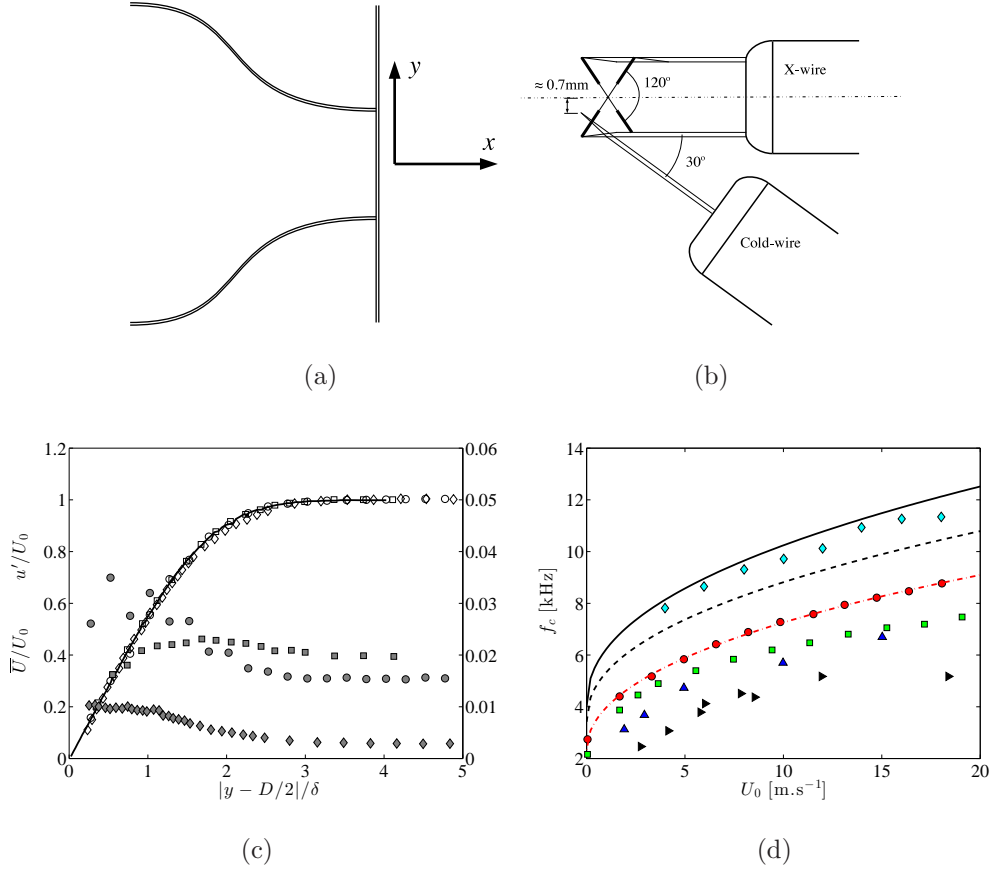


FIG. 1. (a) Sketch of the jet facility and coordinate system. (b) Schematic of the hot-cold wire probe used for the present measurements. (c) Mean velocity (open symbols) and rms profiles (closed symbols) near the jet exit. \circ present measurements, \square data from Burattini *et al.*³⁴, \diamond data from Hussain & Clark³⁵, — Blasius profile. (d) Cut-off frequency of the cold wire measured using a square wave current injection. \circ present measurements with a Pt $0.6\mu\text{m}$ wire probe, \square present measurements with a Pt-10%Rh $0.63\mu\text{m}$ wire probe, \diamond data from Lemay & Benaïssa⁴⁰ with a Pt-10%Rh $0.58\mu\text{m}$ wire probe submitted to the current injection test, \triangle data from Fiedler⁴¹ using a Pt-10%Rh $0.63\mu\text{m}$ wire probe and a chopped laser beam, \triangleright data from Antonia *et al.*⁴² using a Pt-10%Rh $0.63\mu\text{m}$ wire probe and the pulsed wire technique. — and - - - correspond to the theoretical expectations for a Pt $0.6\mu\text{m}$ and a Pt-10%Rh $0.63\mu\text{m}$ wire respectively and — · — is the fit using the functional $f_c = A_1 + A_2\sqrt{U_0} + A_3U_0$, with $A_1 = 2.06$, $A_2 = 1.70$ and $A_3 = -0.18$.

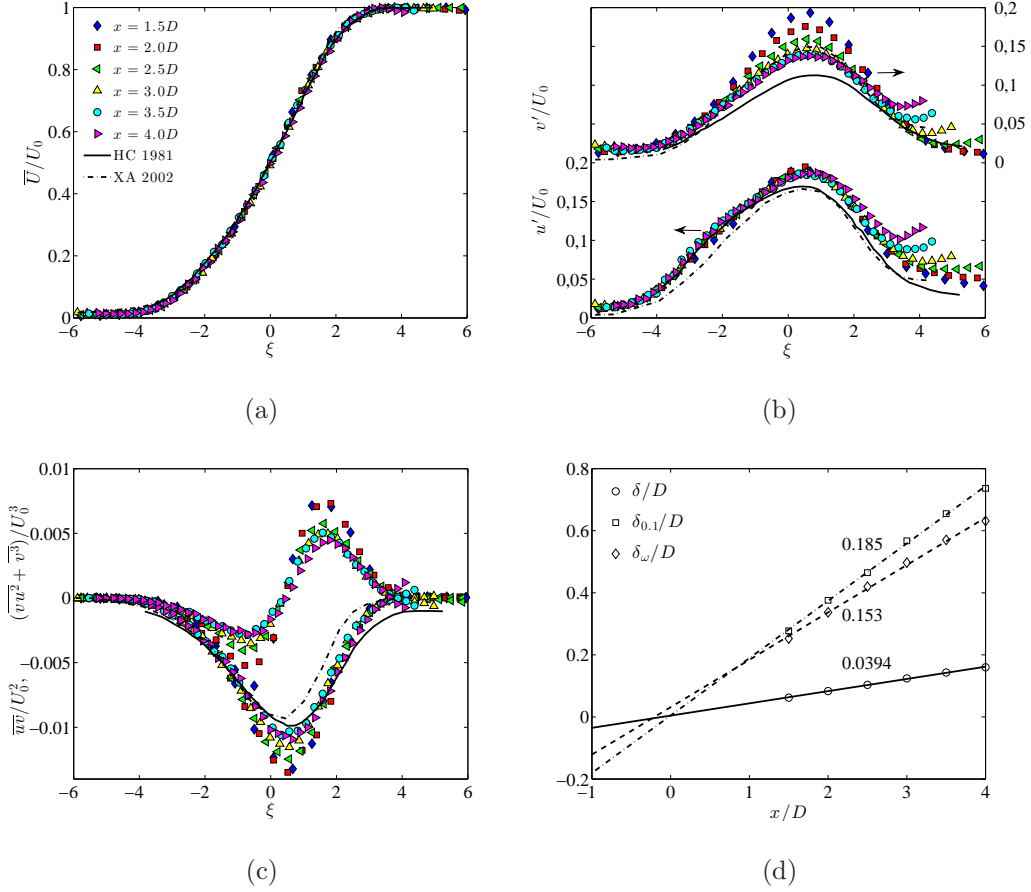


FIG. 2. Profiles of (a) mean velocities, (b) rms, (c) higher order statistics, as a function of the normalized transverse distance ξ for different downstream positions. $\diamond x = 1.5D$, $Re_\delta = 2.8 \times 10^3$. $\square x = 2D$, $Re_\delta = 3.7 \times 10^3$. $\triangleleft x = 2.5D$, $Re_\delta = 4.6 \times 10^3$. $\triangle x = 3D$, $Re_\delta = 5.5 \times 10^3$. $\circ x = 3.5D$, $Re_\delta = 6.4 \times 10^3$. $\triangleright x = 4D$, $Re_\delta = 7.2 \times 10^3$. — Hussain & Clark³⁵ and - - - Xu & Antonia⁴⁴. (d) Streamwise evolution of the shear layer length-scales δ , $\delta_{0.1}$ and δ_ω together with their respective linear fit (lines).

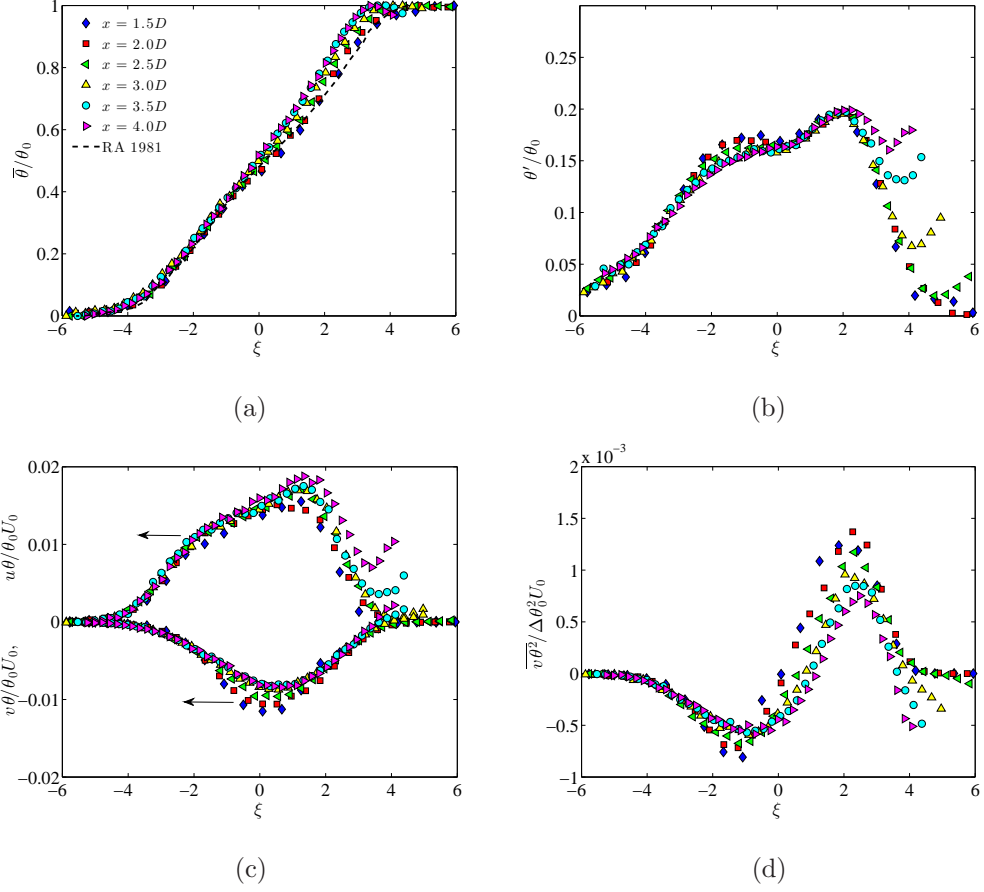


FIG. 3. Profiles of (a) mean scalar values, (b) rms of scalar fluctuations, (c) and (d) velocity-scalar correlations as a function of the normalized transverse distance ξ for different downstream positions. See Fig. 2(a) for legend. In (a) - - - corresponds to the data of Rajagopalan & Antonia⁴⁵ obtained in the shear layer of a heated plane jet.

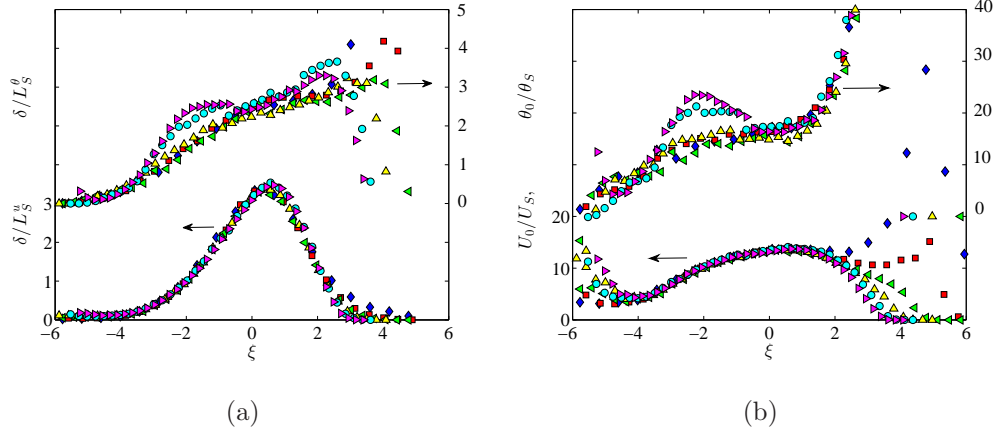


FIG. 4. (a) Profiles of δ/L_S^u and δ/L_S^θ , with the shear length-scales $L_S^u \equiv \sqrt{\bar{\epsilon}/S_u^3}$ and $L_S^\theta \equiv \sqrt{\bar{\epsilon}_\theta^{3/2}/\bar{\epsilon}^{1/2}S_\theta^3}$. (a) Profiles of the shear characteristic velocity $U_S = \sqrt{\bar{\epsilon}/S_u}$ and characteristic temperature $\theta_S = \bar{\epsilon}_\theta/S_\theta\sqrt{S_u/\bar{\epsilon}}$. See Fig. 2(a) for legend.

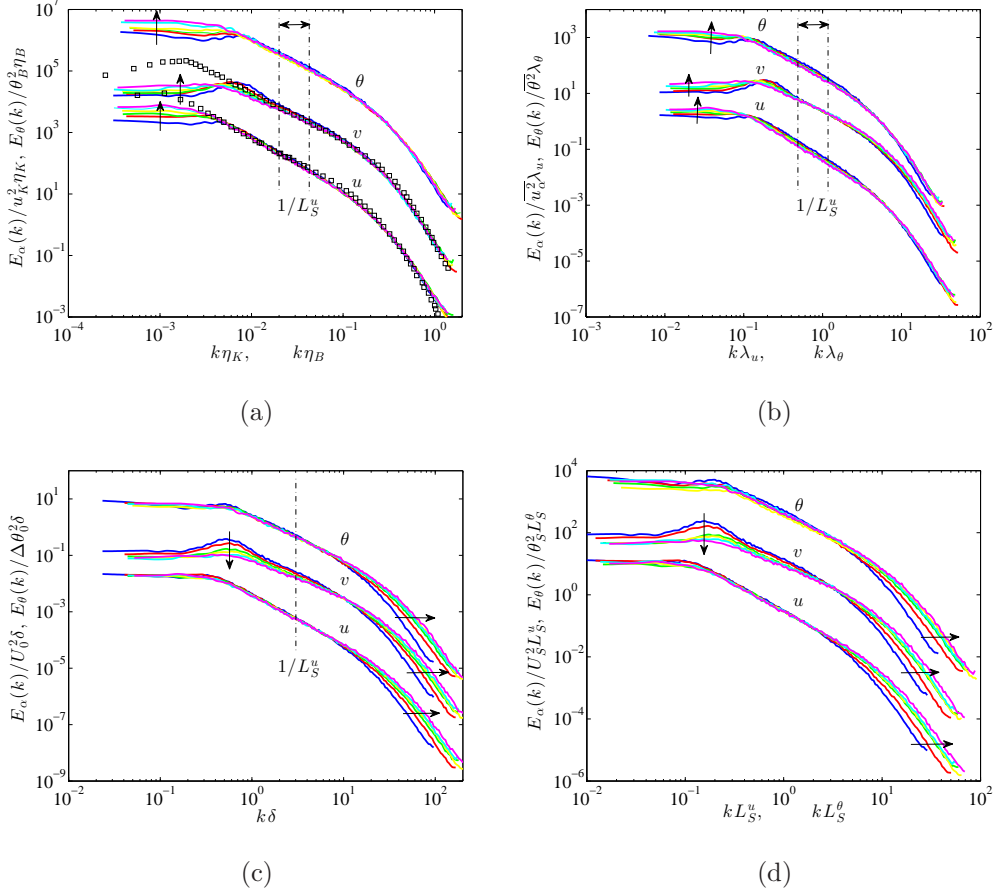


FIG. 5. Spectra in the range $1.5D \leq x/D \leq 4D$, normalized by (a) either Kolmogorov (u_K, η_K) or Batchelor scales (θ_B, η_B), (b) George similarity variables ($\overline{u_\alpha^2}, \lambda$), ($\overline{\theta^2}, \lambda_\theta$), (c) outer variables δ and either U_0 or θ_0 , (d) shear length-scales (L_S^u, U_S) or (L_S^θ, θ_S). Spectra of v and θ are shifted upwards by a factor of 25 and 25^2 respectively. The arrows indicate the direction of increasing x . In (a) square symbols correspond to the spectra measured by Ref. 33 in the plane shear layer

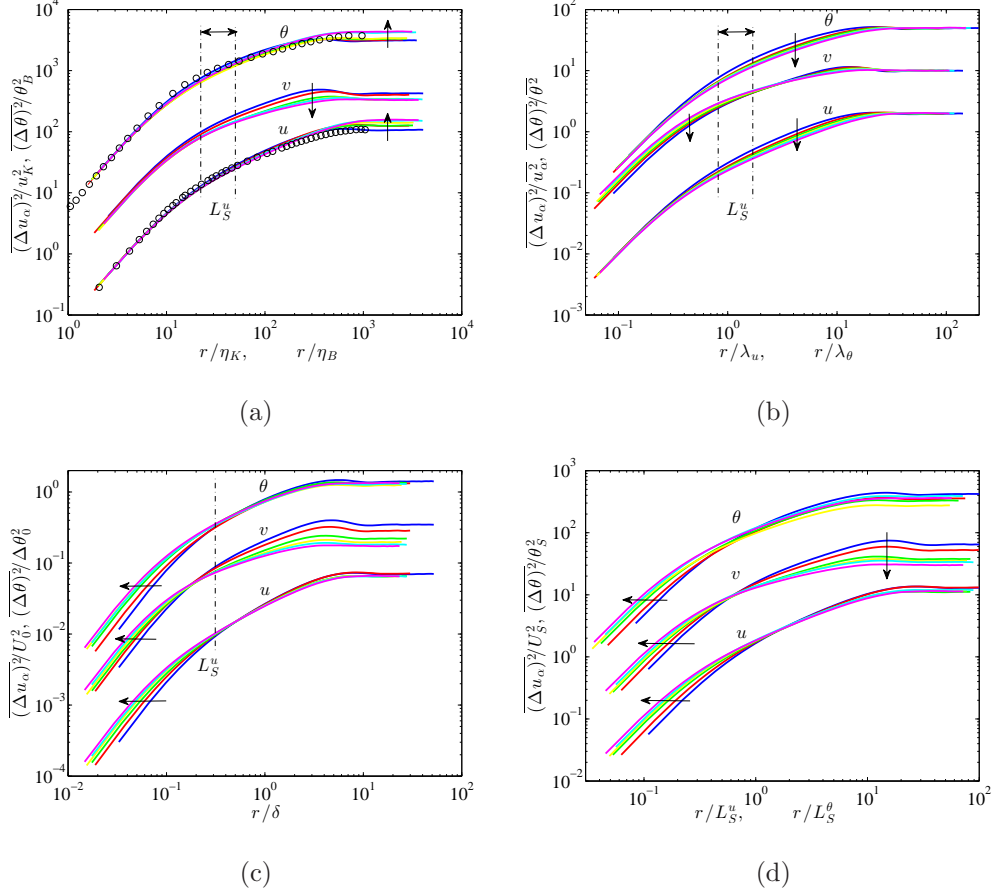


FIG. 6. Second-order structure functions in the range $1.5D \leq x/D \leq 4D$, normalized by (a) either Kolmogorov (u_K, η_K) or Batchelor scales (θ_B, η_B), (b) George similarity variables ($\overline{u_\alpha^2}, \lambda$), ($\overline{\theta^2}, \lambda_\theta$), (c) outer variables δ and either U_0 or θ_0 , (d) shear length-scales (L_S^u, U_S) or (L_S^θ, θ_S). Structure function of v and θ are shifted upwards by a factor of 5 and 25 respectively. The arrows indicate the direction of increasing x . In (a) the symbols correspond to the data of Refs. 53 and 54

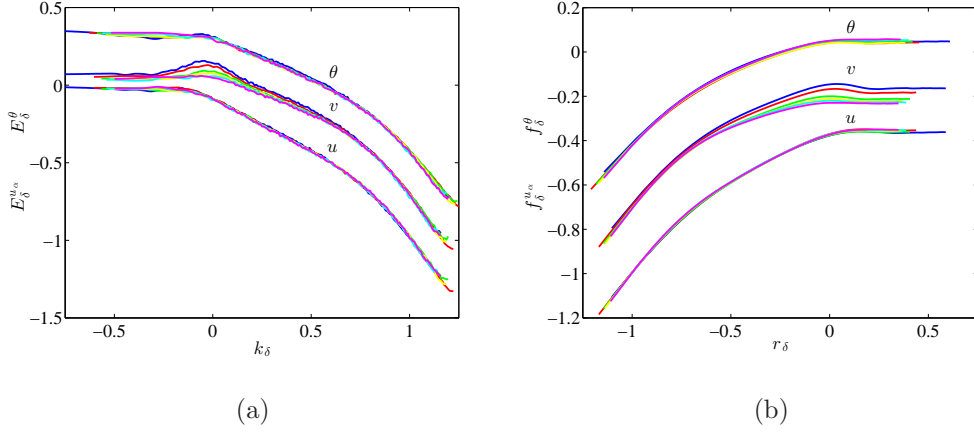


FIG. 7. Log-similarity for the energy spectra and structure functions. (a) Energy spectra with $C_1 = 0.25$ and $C_2 = 1$, spectra of v and θ are shifted upwards by factors of 0.2 and 0.4 respectively. (b) structure functions with $C_1 = 0.25$ and $C_2 = 1$, structure functions of v and θ are shifted upwards by factors of 0.2 and 0.4 respectively.